FRONTIERS OF PHYSICS

RESEARCH ARTICLE
Volume 18 / Issue 5 / 53301 / 2023

Overcoming Debye length limitations: Three-dimensional wrinkled graphene field-effect transistor for ultra-sensitive adenosine triphosphate detection

Yue Ding[1,2], Chonghui Li[2,3,†], Meng Tian[1,2], Jihua Wang[2,3], Zhenxing Wang[2], Xiaohui Lin[2,3], Guofeng Liu[2], Wanling Cui[2,3], Xuefan Qi[2], Siyu Li[2], Weiwei Yue[1,‡], Shicai Xu[2,3,§]

1 School of Physics and Electronics, Shandong Normal University, Jinan 250014, China
2 Shandong Key Laboratory of Biophysics, Institute of Biophysics, Dezhou University, Dezhou 253023, China
3 Shandong Engineering Laboratory of Swine Herd Health Big Data and Intelligent Monitoring, Dezhou University, Dezhou 253023, China
Corresponding authors. E-mail: †chlisdnu@126.com, ‡yuewei@sdnu.edu.cn, §shicaixu@dzu.edu.cn
Received December 5, 2022; accepted March 11, 2023

ABSTRACT

Adenosine triphosphate (ATP) is closely related to the pathogenesis of certain diseases, so the detection of trace ATP is of great significance to disease diagnosis and drug development. Graphene field-effect transistors (GFETs) have been proven to be a promising platform for the rapid and accurate detection of small molecules, while the Debye shielding limits the sensitive detection in real samples. Here, a three-dimensional wrinkled graphene field-effect transistor (3D WG-FET) biosensor for ultra-sensitive detection of ATP is demonstrated. The lowest detection limit of 3D WG-FET for analyzing ATP is down to 3.01 aM, which is much lower than the reported results. In addition, the 3D WG-FET biosensor shows a good linear electrical response to ATP concentrations in a broad range of detection from 10 aM to 10 pM. Meanwhile, we achieved ultra-sensitive (LOD: 10 aM) and quantitative (range from 10 aM to 100 fM) measurements of ATP in human serum. The 3D WG-FET also exhibits high specificity. This work may provide a novel approach to improve the sensitivity for the detection of ATP in complex biological matrix, showing a broad application value for early clinical diagnosis and food health monitoring.

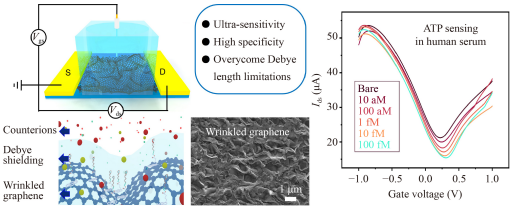

Keywords ATP in complex human serum, three-dimensional wrinkled graphene, field effect transistor, Debye shielding, ultra-sensitive

1 Introduction

Adenosine triphosphate (ATP), as a kind of high-energy compound, exists in all life stages of higher animals and plants, and plays an important role in maintaining the normal function of organisms [1, 2]. Meanwhile, the continuous fluctuation of the ATP concentration level can reflect the energy charge state of the cell [3], which is closely related to the development mechanism of certain diseases, such as therioma, alzheimer, and acute kidney injury [4–8]. At present, the detection methods of ATP mainly include electrochemical method, high performance liquid chromatography, isotope tracer method, and so on [9–11]. These above detection methods offer considerable assistance for all-electrical detection of

Higher Education Press

https://doi.org/10.1007/s11467-023-1281-7

ATP, but they still suffer from insurmountable disadvantages such as high costs, the complexity of the synthesis process, the need for label probes, and the influence of common interfering substances. Therefore, simple, rapid, sensitive and accurate detection of ATP has important practical significance.

Biological sensors based on field-effect transistors (FETs) convert biological signals into measurable electrical signals, which are applied in various fields with their miniaturization, label-free, low cost and can be readily integrated with other electronic components [12]. Among all kinds of FETs, graphene field-based effect transistors (G-FETs) have been widely used in biosensing, environmental monitoring and disease diagnosis [13–18] because of graphene's superior structural properties and physical chemical properties, such as large surface-to-volume ratio, high electrical conductivity and carrier mobility, excellent biological compatibility and flexibility [19–22]. By now, ATP sensors have been developed somewhat. For example, Souvik *et al.* [23] reported an FET-like electrochemical nano-biosensor employing monolayer graphene as the conducting channel to detect ATP, achieving a detection limit as low as 10 pM. Earlier, our group integrated multilayer large-area graphene with FETs, and selected ATP as a detection electrolyte, showing a good correlation with ATP concentration from 10 pM to 10 μM [24]. Despite the impressive achievements of flat graphene FET sensors, most G-FETs struggle to achieve ultra-sensitive detection in complex environments [25–29]. One reason is the impact of the Debye limitations. The Debye shielding is a phenomenon of counterions shielding in solution on the molecular charge. The extent of shielding is characterized by the Debye length, which is < 1 nm in physiological fluids [30, 31]. Beyond the Debye length limitations, the interactions between the charges are electrically screened, while most biomolecules are larger than 1 nm in size [30]. Thus, an important method to further improve the detection sensitivity of biomolecules can be achieved by overcoming Debye length limitations.

Recently, graphene-conductive channels in the FET biosensors have been innovatively fabricated as a macroscopic three-dimensional framework based on flexible and stretchable substrates (polystyrene, polyimide) or holey structures (foam Ni, gels, Cu) [32–37]. Based on the inherent properties of two-dimensional graphene, 3D graphene not only provides higher number of active adsorption sites, but also overcomes Debye length limitations, which provides an opportunity to realize ultra-sensitive detection of charged biomolecules.

Here, we fabricated a three-dimensional wrinkled graphene FET sensor, achieving ultra-sensitive and high-specific detection of ATP molecules. The wrinkled graphene is achieved by the shrinkage of 2D layer plastic substrate, while allowing facile fabrication. The novel device with unique graphene morphology enables ultra-sensitive detection of ATP by overcoming Debye length limitations. The limit of detection (LOD) of the sensor for analyzing ATP is as low as 3.01 aM in buffer and 10 aM in human serum, far lower than traditional detection methods. Meanwhile, the 3D WG-FET sensor shows a good linear electrical response to logarithm of ATP concentrations in both buffer and complex biological matrix. The successful measurements of the trace ATP in human serum indicate the promising development potential for ATP sensors in real samples. The sensor has almost no response to ATP analogs, indicating the high specificity of 3D WG-FET. Based on 3D WG-FET, we have achieved ultra-sensitive detection of ATP in a complex environment, which probably has broad application prospects in the field of point-of-care testing.

2 Materials and methods

2.1 Materials

Polystyrene (PS, 50 nm thick) was purchased from Tianzheng JD.COM as a substrate for 3D WG-FET fabrication. The Cu foil (99.999%, 200 mm thick) was purchased from Alfa Aesar (China). ATP, guanosine-5'-triphosphate (GTP), cytidine-5'-triphosphate (CTP), and uridine-5'-triphosphate (UTP) were purchased from Solarbio as test samples. ATP aptamer (5'-N_2H-AAC CTG GGG GAG TAT TGC GGA GGA AGG T-3') was purchased from Sangon Biotech. 1-pyrenebutanoic acid succinimidyl ester (PBASE) and ethanolamine were purchased from Sigma-Aldrich. Simethyl sulfoxide was purchased from Macklin. Normal human serum was purchased from Solarbio. All salts were purchased from Sigma-Aldrich and dissolved in deionized water.

2.2 Fabrication of the 3D WG-FET biosensor

The single-crystal graphene was grown by chemical vapor deposition (CVD). A piece of Cu foil (10 cm × 10 cm × 200 mm) was ultrasonicated in acetone, methanol, and deionized water (with each solvent successively for 10 min) to remove impurities. The Cu foil was then placed into the CVD quartz reaction chamber. After that, the quartz reaction chamber was evacuated to 2.5×10^{-5} Pa, and H_2 (99.999%) was introduced at a 50 sccm flow rate to clean the Cu foil surface for graphene nucleation. After 100 minutes, CH_4 (99.999%, 40 sccm) was mixed into H_2 in the chamber and graphene was grown at 1000 °C for half an hour.

We designed a 3D WG-FET sensor to detect ATP, and the main step was to create a 3D WG sensing channel. The schematic diagram of the 3D WG-FET experimental fabrication is shown in Fig. 1(a). First, the Cu foil with single-crystal graphene was cut into small pieces of 2 cm × 2 cm with scissors. The Cu foil was then etched by floating on 0.1 M $FeCl_3$ aqueous. The

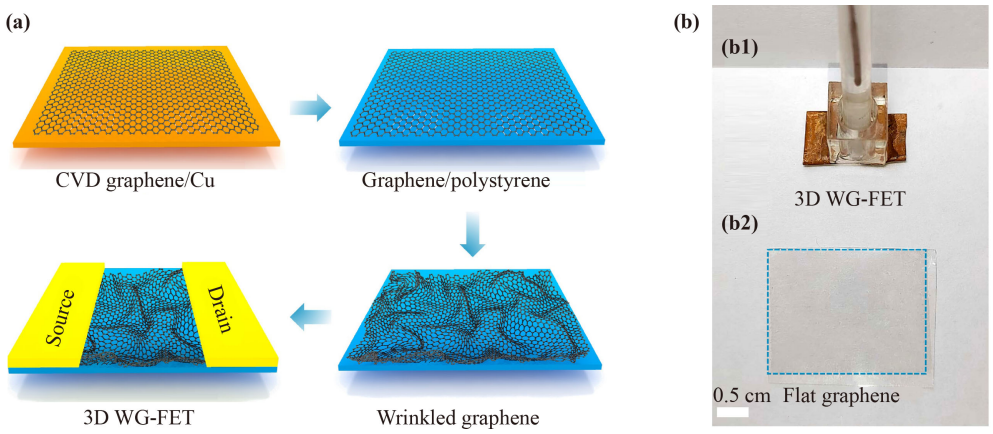

Fig. 1 Fabrication of 3D WG-FET. **(a)** Schematic diagram of the 3D WG-FET experimental fabrication. **(b)** The photo of 3D WG-FET and flat graphene.

graphene was rinsed by moving from $FeCl_3$ aqueous to deionized water three times and then transferred onto the polystyrene substrate. Through a simple annealing process (120 °C, 1 h), the graphene/polystyrene substrate [Fig. 1(b2)] shrank to about a quarter of its original size [38]. Gold was sputtered to prepare source and drain electrodes of 3D WG-FET sensor by magnetic sputtering (100 W, 45 s). The device was then encapsulated in PMMA (8 mm × 8 mm × 8 mm), leaving an open cavity over the graphene conducting channel for biological sample placement. The Ag/AgCl electrode was placed above the WG channel and was used as a gate electrode of the 3D WG-FET device for gate voltage scan. The photo of the fabricated 3D WG-FET device with a PMMA sample pool is shown in Fig. 1(b1).

2.3 Functionalization of the 3D WG-FET biosensor

To immobilize the ATP aptamers onto the 3D WG surface without introducing defects, the PBASE linkers were introduced to fix aptamers onto the whole surface of WG. 100 mM PBASE solution dissolved in dimethyl sulfoxide (DMSO) was introduced into the sample pool to modify WG for 10 h at room temperature. The pyrenyl group of PBASE was closely linked to the basal plane of pristine graphene via π–π stacking. The WG was then sequentially rinsed with DMSO, ethanol, and 1 × PBS to wash away any excess reagents. Then, 10 μM 5'-amine-modified ATP aptamer dissolved in 1 × PBS buffer was injected into the sample pool to modify the PBASE/WG for 12 h at room temperature. The amino group at the end of the 5' end of the ATP aptamer reacted strongly with the succinimide part of PBASE to form a stable amide bond. Later, the sample was washed thoroughly with buffer to remove the non-bound aptamer. 100 mM ethanolamine solution was soaked into the sample pool for 1 h to deactivate and block the unreacted groups on the WG surface.

2.4 Detection of ATP

After functionalization, 1 × PBS buffer solution was introduced instead of ethanolamine, and then ATP solutions with different concentrations were injected onto the 3D WG-FET channel to conduct electrical measurements. After exposure to the ATP solutions for 40 minutes, the transfer curves were recorded, and the device was thoroughly washed for the next measurement. The volume of all treated chemicals and samples was 35 μL. To measure the transfer characteristics of the 3D WG-FET sensor, the drain voltage (V_{ds}) was set to 100 mV. The gate voltage (V_{gs}) varied from –1 to 1 V with a scanning step of 30 mV. The charge neutrality point voltage (V_{cnp}) is at the minimum conductance point of the transfer characteristic curve. The measurements were repeated at least three times to ensure the stability of V_{cnp} during the measurement process.

2.5 Characterizations and electronic measurements

The morphologies of 3D WG were characterized by scanning electron microscopy (SEM, ZEISS Merlin compact) and Atomic Force Microscope (AFM, Multimode 8-HR). The graphene and PS were characterized using a Raman spectrometer (Horiba HR Evolution) with laser excitation at 532 nm. All electrical measurements were performed using a PDA FS360 analyzer coupled with the probe station PEH-4.

3 Results and discussion

3.1 Characterization of 3D WG-FET device

A scanning electron microscope (SEM) was used to characterize the 3D WG formed by the shrinkage of PS substrate. Figure 2(a) shows a large number of continuous and disordered structures in large-scale SEM, indicating

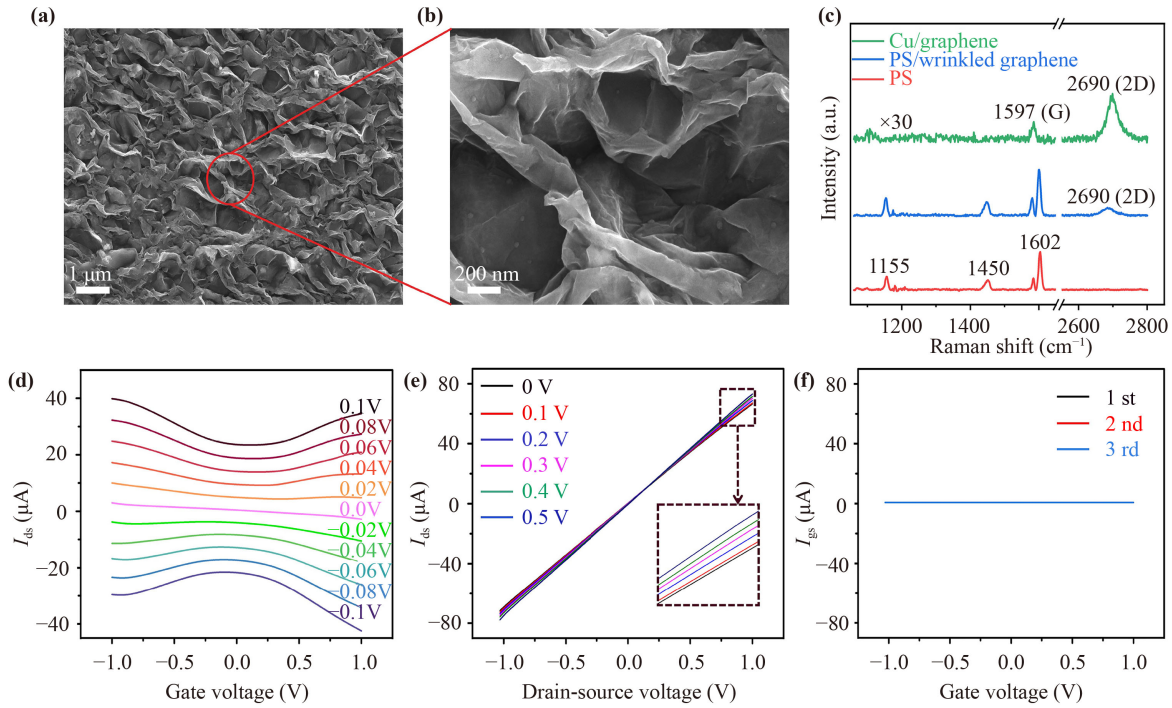

Fig. 2 Characterization of 3D WG-FET. **(a)** Low and **(b)** High-magnification SEM images of WG. **(c)** Raman spectra of Cu/graphene, PS/wrinkled graphene and PS substrate. **(d)** Charge transfer characteristics of 3D WG-FET. **(e)** Transfer output curves of 3D WG-FET. **(f)** The gate current of 3D WG-FET.

that the graphene/PS structure is tightly bound and is not destroyed after heating to shrink into a 3D structure. Further amplification of the scale allows more tiny wrinkles to be observed in Fig. 2(b). The bright stripes like gyrus and sulcus prove that the graphene is successfully transferred to the PS substrate, and also prove that the graphene is not damaged during the heating and wrinkling process, which ensure the high quality of graphene and lay the foundation for the subsequent high-sensitivity detection of 3D WG-FET. The formation of the WG was also verified by atomic force microscopy (AFM), showing the hierarchical wrinkles (Supplementary Fig. S1). Additionally, 3D WG-FET will overcome the Debye limitations, possibly due to these 3D wrinkles. Raman spectra of Cu/graphene, PS/wrinkled graphene and PS are shown in Fig. 2(c). The Raman spectrum collected from flat graphene on a Cu foil [Green curve in Fig. 2(c)] shows typical features of monolayer graphene with the intensity ratio $I_{2D}/I_G \geq 2$ and the D band defect-related is invisible, showing the high quality of graphene [39]. In addition, the red curve in Fig. 2(c) presents the Raman spectrum of the polystyrene substrate. Typical peaks of the PS at 1155, 1450 and 1602 cm^{-1} are observed, corresponding to υ_{15} mode, υ_{19b} or (CH_2), and υ_{12} C–C stretching mode, respectively [40, 41]. After graphene was wet-transferred on PS and then heated for shrinking, there clearly exists the 2D band in the Raman spectrum of PS/wrinkled graphene [Blue curve in Fig. 2(c)] contrast to that of PS, indicating the successful transfer of monolayer graphene from Cu to the PS substrate. Meanwhile, according to the Raman spectrum analysis, the D peak is not observed, indicating the high quality of WG, which is consistent with the results observed by SEM and the Raman spectrum of Cu/graphene. The transfer characteristic curves (drain current versus gate voltage) of 3D WG-FET show a typical ambipolar field effect characteristic, as shown in Fig. 2(d). The Dirac points varies with V_{ds}, which is mainly the work function difference of the graphene and Ag/AgCl gate electrode [39]. Figure 2(e) presents the linear relationship between the drain-source current (I_{ds}) and drain-source voltage (V_{ds}), indicating good ohmic contact between WG and the electrodes. Moreover, the gate-source current (I_{gs}), also known as leakage current, is measured as low as 0.689 μA, further ensuring ultra-sensitive detection of the 3D WG-FET [Fig. 2(f)]. Therefore, the sensor shows typical and excellent field effect characteristics where the electron transport can be modulated by gate voltage (V_{gs}).

3.2 Sensing mechanism of 3D WG-FET device

Figure 3(a) presents the schematic diagram of PBASE, aptemer, ethanolamine and ATP incubation process on WG/PS substrate. To obtain a functional 3D WG-FET sensor, the PBASE and ATP aptamer were successively modified on the surface of graphene, and then hybridized with ATP. The sequences of ATP aptamer

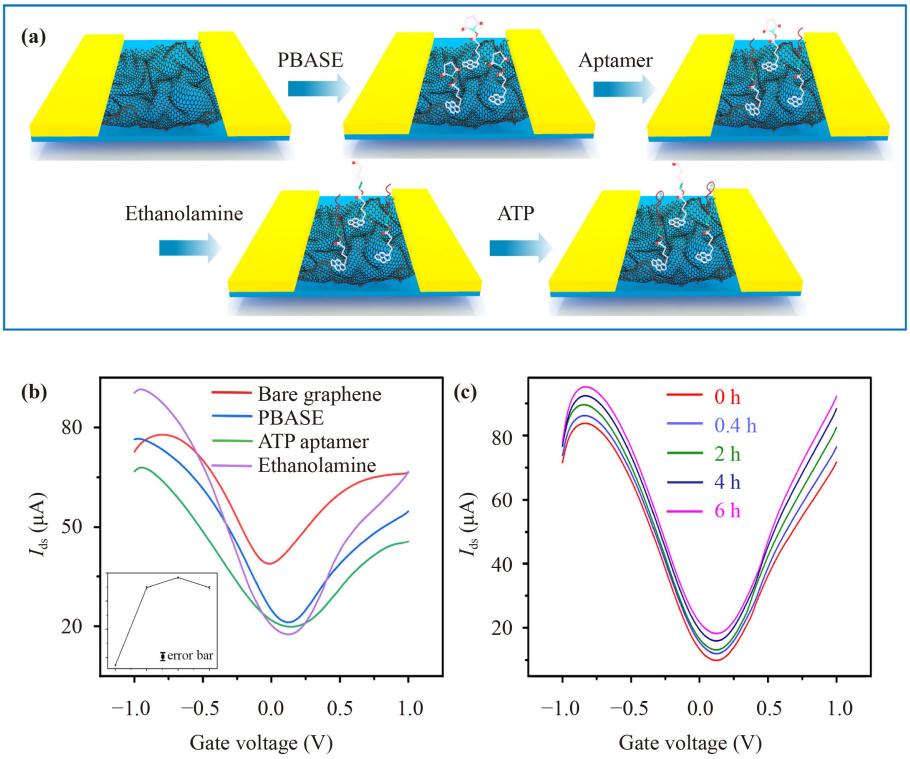

Fig. 3 Functionalization of 3D WG-FET sensor. **(a)** Schematic diagram of PBASE, aptamer, ATP and ethanolamine incubation process on WG/PS, and **(b)** the corresponding transfer characteristics of 3D WG-FET for the above each step. **(c)** The transfer characteristics curve of the probe functionalized sensor in PBS at the given time in the legend.

and the structures of the molecules used in the experiments are shown in Supplementary Fig. S2. Figure 3(b) presents the transfer curves of PBASE, aptamer, ATP and ethanolamine incubation process, accordingly. The intrinsic p-type behavior of the transfer curve [Red curve in Fig. 3(b)] is due to the negatively charged impurities trapped by graphene during the transfer process [42]. Through the stacking force between the pyrene group and the graphene, the linker molecules (PBASE) can bond to the six-membered ring structures of 3D WG [43]. The transfer curve [Blue curve in Fig. 3(b)] is positively shifted after modifying PBASE, which is due to the p-doping effect between graphene and the pyrene group of PBASE [44, 45]. Aptamer can be covalently bonded with PBASE through amide bonds that are generated by combination of the amino group on the aptamer and the succinimide moiety on PBASE [46]. The transfer curve [Green curve in Fig. 3(b)] moves further to the positive gate voltage direction after aptamer modification, which can be explained by the negative electrostatic gating effect [47, 48]. The addition of ethanolamine shifted the Dirac point towards the lower voltage due to eliminating the non-bonded and weakly bonded aptamer and the consequent removal of negative charge [Purple curve in Fig. 3(b)]. ATP can assemble with the aptamer into a stable hairpin structure [49]. ATP containing negatively charged triphosphates regulates the Fermi level through a negative electrostatic gating effect to induce charge migration [50, 51]. The measurements were repeated over time after functionalization and confirmed that the Dirac voltage values were stable in PBS buffer before detecting the ATP solutions. [Fig. 3(c)].

3.3 Sensitivity and specificity of the ATP sensor

After characterizing and functionalizing the 3D WG-FET, the device was then used for ATP sensing. Figure 4(a) shows the transfer characteristic curves of ATP solutions in the concentration range from 10 aM to 10 pM. Meanwhile, each concentration was measured three times to ensure the reliability of the measurement. We can observe that V_{cnp} continuously shifts towards the positive direction as the ATP concentration increases, which can be explained by the negative electrostatic gating effect [51, 52]. Not surprisingly, good linearity (range from 10 aM to 10 pM) between the V_{cnp} changes and the logarithm of ATP concentrations is found, as exhibited in Figure 4b, and the average regression coefficient (R^2) is 0.993, proving the potential for fine quantification. However, the detected signals below 1 aM do not show signal levels which exceed the background threefold, so the relevant data are not valid. The LOD corresponding to a signal-to-noise ratio (S/N) of 3 is calculated to be 3.01 aM. Table 1 compares our

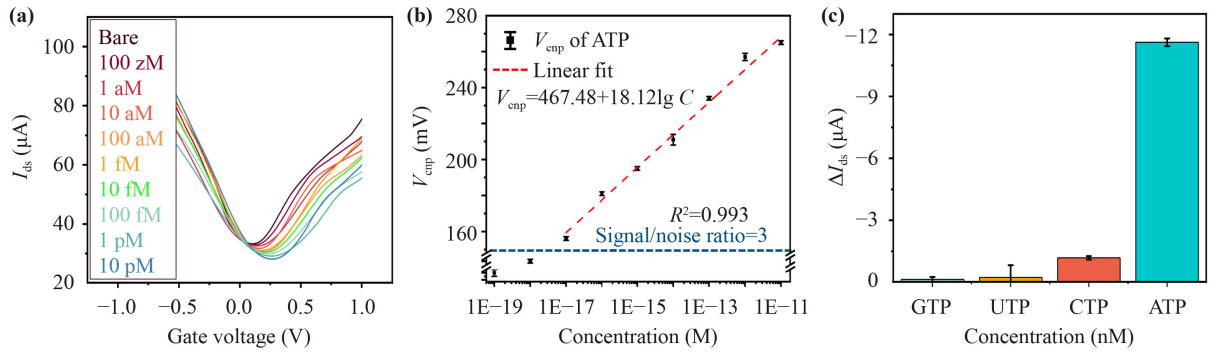

Fig. 4 ATP hybridization detection in PBS buffer using 3D WG-FET. **(a)** Shift of transfer curves of the functionalized 3D WG-FET induced by ATP solution in PBS buffer. **(b)** Linear plot characteristics of V_{cnp} increase versus logarithm of ATP concentrations. **(c)** Specificity of ATP detection comparing with 100 nM ATP analogs (GTP, CTP and UTP).

Table 1 Parameters of different types of ATP sensors.

Sensor type	Limit of detection (LOD)	Sensitive region	Ref. (Year)
Fluorescence	53 nM	0–100 μM	[57] (2022)
Fluorescence	35 nM	0.1–10 μM	[58] (2020)
Colorimetry	8.2 nM	25–600 nM	[59] (2018)
Colorimetry	90 nM	0.5–100 μM	[60] (2019)
Electrochemistry	0.3 nM	5.0–1000 nM	[61] (2022)
Electrochemistry	0.6 nM	1.0–3000 μM	[62] (2017)
Graphene capacitive type biosensor	200 nM	200–800 nM	[53] (2013)
Graphene field-effect transistor	1 μM	1 μM–1 mM	[63] (2022)
Graphene field-effect transistor	10 pM	10 pM–10 μM	[24] (2014)
Graphene field-effect transistor	0.002 mM	0.002–5 mM	[54] (2014)
Graphene foam field-effect transistor	0.5 pM	0.5 pM–50 μM	[51] (2018)
3D wrinkled graphene field-effect transistor	3.01 aM	10 aM–10 pM	This work

proposed 3D WG-FET with other sensors for detecting ATP reported previously, and the result turns out to be that the LOD of 3D WG-FET is far lower than those reported results. Our group has also done a lot of experiments about flat graphene sensor for ATP detection. Yue *et al.* [53] fabricated a capacitive type biosensor based on large-area multilayer graphene produced by chemical vapor deposition, achieving ATP detection with concentration from 200 nM to 800 nM. After that, we fabricated an integrated field effect transistor integrated with graphene field-effect transistors (FETs) and achieved high sensitivity to detect ATP as low as 10 pM [24]. Xu *et al.* [54] directly synthesized continuous, uniform graphene films on quartz substrates using a two-temperature-zone chemical vapor deposition system, and their layers can be controlled by adjusting the precursor partial pressure, showing a fast and high-sensitive to ATP molecules over a very wide range from 0.002 to 5 mM. Our group also fabricated a sensitive and selective graphene foam field-effect transistor to detect ATP, achieving reproducible and low detection limit as low as 0.5 pM [51]. The surface structure of 3D materials could affect the electrostatic interaction at the solid-liquid interface [55]. Using numerical simulations, Shoorideh *et al.* [56] showed that the enhanced sensitivity observed in nanoscale biosensors because electrostatic screening is weaker in the vicinity of concave curved surfaces and stronger in the vicinity of convex surfaces. Hwang *et al.* [38] applied to texture 2D materials to prepare the FET sensor. Nanoscale crumples of graphene perturbed EDL in ionic solutions and resulted in higher detection sensitivity due to reduced Debye screening effect. Meanwhile, computational simulations also confirmed this. The ultra-sensitivity of the 3D WG-FET sensor is attributed to overcoming Debye length limitations, which results in more exposure of the ATP molecules to the recognition interface. The Debye length modulation concept before and after the crumpling process is interpreted in Supplementary Fig. S3. The blue interface represents the Debye length limitations in solution. Before the crumpling process, the constraint of counterions is weak and ions uniformly distribute on the surface of flat graphene, resulting in a constant Debye length. However, because of the confined nature of the concave region [35], ions

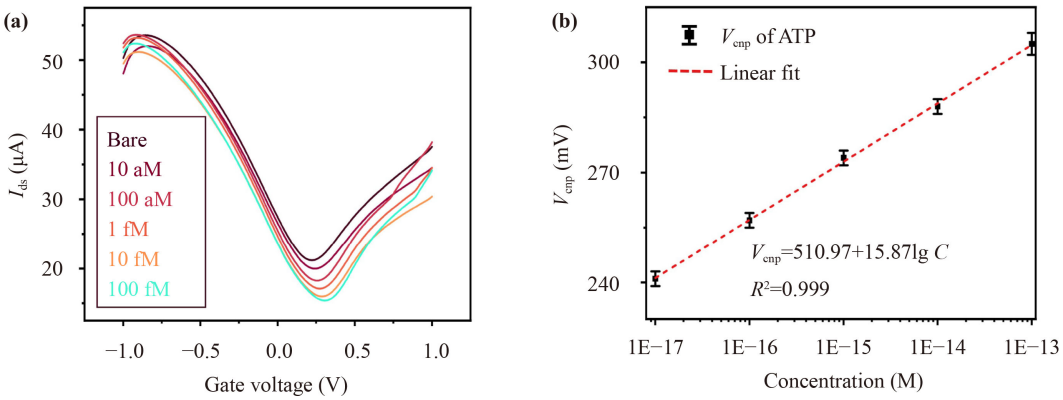

Fig. 5 ATP hybridization test in 10% diluted human serum using 3D WG-FET. **(a)** Shift of transfer curves of the functionalized 3D WG-FET induced by ATP solution in 10% diluted human serum samples. **(b)** Linear plot characteristics of V_{cnp} increase versus logarithmic changes in ATP concentration.

are excluded, the screening by ions is farther away from the concave graphene surface leading to much of the ATP charges unscreened next to the graphene surface. It changes the graphene carrier density, overcoming Debye length limitations and achieving ultra-sensitive detection. Besides sensitivity, specificity is also a key parameter in evaluating the performance of FET biosensors. The specificity was verified by comparing the signals elicited by ATP as well as its analogues (UTP, GTP, and CTP). As shown in Fig. 4(c), only the addition of ATP causes obvious current changes, while the signal responses of other analogues are relatively small and negligible under the same concentration. The results confirm that the ATP sensing of 3D WG-FET is not interfered by GTP, CTP and UTP.

3.4 ATP analysis in human serum

To evaluate the capability to detect ATP in complex biological matrices, we tried to apply 3D WG-FET biosensors in human serum samples. Figure 5(a) presents the measured transfer characteristic curves of 3D WG-FET after loading a series of ATP standard solutions (10 aM to 100 fM) containing 10% diluted human serum. The transfer curves of the functionalized 3D WG-FET for ATP detection behave similarly to those obtained in buffer. Figure 5(b) shows a good linear relationship, which is represented by $V_{cnp} = 510.97+15.87\lg\ C$ ($R^2 = 0.999$). The error bars suggest that the device has good repeatability in 10% diluted human serum. These results illustrate that our proposed 3D WG-FET has the potential to realize the detection of trace ATP in other biological systems in the future.

4 Conclusion

In summary, we fabricated a novel three-dimensional wrinkled graphene FET formed by the shrinkage of plastic substrate for ultra-sensitive and high-specific analysis of the small biomolecule ATP in both matrixes. Benefiting from the 3D graphene channel, the biosensor overcomes the Debye length limitations in ionic solution and shows unprecedented sensitivity to ATP, with LOD as low as 3.01 aM in PBS and 10 aM in human serum. The 3D WG-FET biosensor also shows a good linear electrical response to logarithm of ATP concentrations in both buffer and complex biological matrix, indicating the application potential of the sensor in the quantitative detection of ATP. Moreover, the 3D WG-FET biosensor shows high specificity, which allows the detection of trace ATP in real samples full of various of matrixes. The 3D WG-FET sensor could be further developed to detect trace macromolecules whose size exceeds the Debye length limitations in living cells and even organisms.

Electronic supplementary materials The online version contains supplementary material available at https://doi.org/10.1007/s11467-023-1281-7 and https://journal.hep.com.cn/fop/EN/10.1007/s11467-023-1281-7.

Acknowledgements We are grateful for financial support from the National Natural Science Foundation of China (Nos. 12274058 and 12104085), Taishan Scholars Program of Shandong Province (No. tsqn201812104), the Natural Science Foundation of Shandong Province (No. ZR2021QA008), the Qingchuang Science and Technology Plan of Shandong Province (No. 2019KJJ017), and the project of the Talent Introduction of Dezhou University (No. 2021xjrc101).

References

1. F. Di. Virgilio, A. C. Sarti, S. Falzoni, E. De. Marchi, and E. Adinolfi, Extracellular ATP and P2 purinergic signalling in the tumour microenvironment, *Nat. Rev. Cancer* 18(10), 601 (2018)
2. Y. Xu, Q. Kang, B. Yang, B. Chen, M. He, and B. Hu,

A nanoprobe based on molybdenum disulfide nanosheets and silver nanoclusters for imaging and quantification of intracellular adenosine triphosphate, *Anal. Chim. Acta* 1134, 75 (2020)
3. J. Deng and A. Walther, ATP-responsive and ATP-fueled self-assembling systems and materials, *Adv. Mater.* 32(42), 2002629 (2020)
4. C. H. Wang, Y. Zhang, W. Tang, C. Wang, Y. K. Han, L. Qiang, J. W. Gao, H. Liu, and L. Han, Ultrasensitive, high-throughput and multiple cancer biomarkers simultaneous detection in serum based on graphene oxide quantum dots integrated microfluidic biosensing platform, *Anal. Chim. Acta* 1178, 338791 (2021)
5. L. Xiao, K. Li, B. Z. Liu, J. Y. Tu, T. X. Li, Y. T. Li, and G. J. Zhang, A pH-sensitive field-effect transistor for monitoring of cancer cell external acid environment, *Talanta* 252, 123764 (2023)
6. T. N. Seyfried, G. Arismendi-Morillo, P. Mukherjee, and C. Chinopoulos, On the origin of ATP synthesis in cancer, *iScience* 23(11), 101761 (2020)
7. P. P. Sun, H. C. Chen, S. Y. Lu, J. Hai, W. T. Guo, Y. H. Jing, and B. D. Wang, Simultaneous sensing of H_2S and ATP with a two-photon fluorescent probe in Alzheimer's disease: Toward understanding Why H_2S regulates glutamate-induced ATP dysregulation, *Anal. Chem.* 94(33), 11573 (2022)
8. K. M. Dwyer, B. K. Kishore, and S. C. Robson, Conversion of extracellular ATP into adenosine: A master switch in renal health and disease, *Nat. Rev. Nephrol.* 16(9), 509 (2020)
9. Y. Liu, L. Q. Kong, H. Li, R. Yuan, and Y. Q. Chai, Electrochemical aptamer biosensor based on ATP-induced 2D DNA structure switching for rapid and ultrasensitive detection of ATP, *Anal. Chem.* 94(18), 6819 (2022)
10. L. Peng, J. Zhou, G. Liu, L. Yin, S. Ren, S. Man, and L. Ma, CRISPR-Cas12a based aptasensor for sensitive and selective ATP detection, *Sensor Actuat B-Chem.* 320, 128164
11. L. L. Yao, W. J. Zhang, C. X. Yin, Y. B. Zhang, and F. J. Huo, A tracer-type fluorescent probe for imaging adenosine triphosphate under the stresses of hydrogen sulfide and hydrogen peroxide in living cells, *Analyst (Lond.)* 147(19), 4222 (2022)
12. X. Chen, Y. Liu, X. Fang, Z. Li, H. Pu, J. Chang, J. Chen, and S. Mao, Ultratrace antibiotic sensing using aptamer/graphene-based field-effect transistors, *Biosens. Bioelectron.* 126, 664 (2019)
13. I. Park, J. Lim, S. You, M. T. Hwang, J. Kwon, K. Koprowski, S. Kim, J. Heredia, S. A. S. Ramirez, E. Valera, and R. Bashir, Detection of SARS-CoV-2 virus amplification using a crumpled graphene field-effect transistor biosensor, *ACS Sens.* 6(12), 4461 (2021)
14. B. Kwon, H. Bae, H. Lee, S. Kim, J. Hwang, H. Lim, J. H. Lee, K. Cho, J. Ye, S. Lee, and W. H. Lee, Ultrasensitive N-channel graphene gas sensors by nondestructive molecular doping, *ACS Nano* 16(2), 2176 (2022)
15. J. W. Gao, C. H. Wang, C. Wang, Y. J. Chu, S. Wang, M. Y. Sun, H. Ji, Y. K. Gao, Y. H. Wang, Y. K. Han, F. T. Song, H. Liu, Y. Zhang, and L. Han, Poly-L-lysine-modified graphene field-effect transistor biosensors for ultrasensitive breast cancer miRNAs and SARS-CoV-2 RNA detection, *Anal. Chem.* 94(3), 1626 (2022)
16. T. Zhang, S. Wu, R. Yang, and G. Zhang, Graphene: Nanostructure engineering and applications, *Front. Phys.* 12(1), 127206 (2017)
17. X. Chen, S. Hao, B. Zong, C. Liu, and S. Mao, Ultraselective antibiotic sensing with complementary strand DNA assisted aptamer/MoS_2 field-effect transistors, *Biosens. Bioelectron.* 145, 111711 (2019)
18. J. Li, D. Wu, Y. Yu, T. X. Li, K. Li, M. M. Xiao, Y. R. Li, Z. Y. Zhang, and G. J. Zhang, Rapid and unamplified identification of COVID-19 with morpholino-modified graphene field-effect transistor nanosensor, *Biosens. Bioelectron.* 183, 113206 (2021)
19. S. Islam, S. Shukla, V. K. Bajpai, Y. K. Han, Y. S. Huh, A. Ghosh, and S. Gandhi, Microfluidic-based graphene field effect transistor for femtomolar detection of chlorpyrifos, *Sci. Rep.* 9(1), 276 (2019)
20. S. Mao, J. Chang, H. Pu, G. Lu, Q. He, H. Zhang, and J. Chen, Two-dimensional nanomaterial-based field-effect transistors for chemical and biological sensing, *Chem. Soc. Rev.* 46(22), 6872 (2017)
21. S. K. Tiwari, S. Sahoo, N. Wang, and A. Huczko, Graphene research and their outputs: Status and prospect, *Sci. Adv. Mater Dev.* 5(1), 10 (2020)
22. X. M. Huang, L. Z. Liu, S. Zhou, and J. J. Zhao, Physical properties and device applications of graphene oxide, *Front. Phys.* 15(3), 33301 (2020)
23. S. Mukherjee, X. Meshik, M. Choi, S. Farid, D. Datta, Y. Lan, S. Poduri, K. Sarkar, U. Baterdene, C. E. Huang, Y. Y. Wang, P. Burke, M. Dutta, and M. A. Stroscio, A graphene and aptamer based liquid gated FET-like electrochemical biosensor to detect adenosine triphosphate, *IEEE Trans. Nanobiosci.* 14(8), 967 (2015)
24. W. W. Yue, S. Z. Jiang, S. C. Xu, and C. J. Bai, Fabrication of integrated field-effect transistors and detecting system based on CVD grown graphene, *Sens. Actuators B Chem.* 195, 467 (2014)
25. M. Cheng, J. Yang, X. Li, H. Li, R. Du, J. Shi, and J. He, Improving the device performances of two-dimensional semiconducting transition metal dichalcogenides: Three strategies, *Front. Phys.* 17(6), 63601 (2022)
26. Z. Wang, Z. Hao, S. Yu, C. G. De Moraes, L. H. Suh, X. Zhao, and Q. Lin, An ultraflexible and stretchable aptameric graphene nanosensor for biomarker detection and monitoring, *Adv. Funct. Mater.* 29(44), 1905202 (2019)
27. H. H. Bay, R. Vo, X. C. Dai, H. H. Hsu, Z. M. Mo, S. Cao, W. Y. Li, F. G. Omenetto, and X. C. Jiang, Hydrogel gate graphene field-effect transistors as multiplexed biosensors, *Nano Lett.* 19(4), 2620 (2019)
28. Y. K. Han, Y. R. Han, Y. Z. Huang, C. Wang, H. Liu, L. Han, and Y. Zhang, Laser-induced graphene superhydrophobic surface transition from pinning to rolling for

multiple applications, *Small Methods* 6(4), 2200096 (2022)
29. R. Wang, X. G. Ren, Z. Yan, L. J. Jiang, W. E. Sha, and G. C. Shan, Graphene based functional devices: A short review, *Front. Phys.* 14(1), 13603 (2019)
30. M. Hu, N. Zhang, G. Shan, J. Gao, J. Liu, and R. K. Li, Two-dimensional materials: Emerging toolkit for construction of ultrathin high-efficiency microwave shield and absorber, *Front. Phys.* 13(4), 138113 (2018)
31. N. Nakatsuka, K. A. Yang, J. Abendroth, K. Cheung, X. Xu, H. Yang, C. Z. Zhao, B. W. Zhu, Y. Rim, Y. Yang, P. Weiss, M. Stojanovic, and A. Andrews, Aptamer–field-effect transistors overcome Debye length limitations for small-molecule sensing, *Science* 362(6412), 319 (2018)
32. Z. R. Wang, Z. Hao, C. Yang, H. Wang, C. Huang, Z. Zhao, and Y. L. Pan, Ultra-sensitive and rapid screening of acute myocardial infarction using 3D-affinity graphene biosensor, *Cell Rep. Phys. Sci.* 3(5), 100855 (2022)
33. J. W. Gao, Y. K. Gao, Y. K. Han, J. B. Pang, C. Wang, Y. H. Wang, H. Liu, Y. Zhang, and L. Han, Ultrasensitive label-free MiRNA sensing based on a flexible graphene field-effect transistor without functionalization, *ACS Appl. Electron. Mater.* 2(4), 1090 (2020)
34. F. Zhang, Y. H. Li, J. Y. Li, Z. R. Tang, and Y. J. Xu, 3D graphene-based gel photocatalysts for environmental pollutants degradation, *Environ. Pollut.* 253, 365 (2019)
35. T. Deng, Z. H. Zhang, Y. X. Liu, Y. X. Wang, F. Su, S. S. Li, Y. Zhang, H. Li, H. J. Chen, Z. R. Zhao, Y. Li, and Z. Liu, Three-dimensional graphene field-effect transistors as high-performance photodetectors, *Nano Lett.* 19(3), 1494 (2019)
36. C. Wang, S. X. Yang, H. R. Zhang, L. N. Du, L. Wang, F. Y. Yang, X. Z. Zhang, and Q. Liu, Synthesis of atomically thin GaSe wrinkles for strain sensors, *Front. Phys.* 11, 116802 (2016)
37. Y. Z. Huang, Y. K. Han, J. Y. Sun, Y. Zhang, and L. Han, Dual nanocatalysts co-decorated three-dimensional, laser-induced graphene hybrid nanomaterials integrated with a smartphone portable electrochemical system for point-of-care non-enzymatic glucose diagnosis, *Mater. Today Chem.* 24, 100895 (2022)
38. M. T. Hwang, M. Heiranian, Y. Kim, S. You, J. Leem, A. Taqieddin, V. Faramarzi, Y. Jing, I. Park, A. M. van der Zande, S. Nam, N. R. Aluru, and R. Bashir, Ultra-sensitive detection of nucleic acids using deformed graphene channel field effect biosensors, *Nat. Commun.* 11(1), 1543 (2020)
39. Y. Wang, Z. Ni, T. Yu, Z. X. Shen, H. Wang, Y. Wu, W. Chen, and A. T. S. Wee, Raman studies of monolayer graphene: The substrate effect, *J. Phys. Chem. C.* 112(29), 10637 (2008)
40. N. Itoh and N. Hanari, Development of a polystyrene reference material for raman spectrometer (NMIJ RM 8158-a), *Anal. Sci.* 37(11), 1533 (2021)
41. X. X. Zhou, R. Liu, L. T. Hao, and J. F. Liu, Identification of polystyrene nanoplastics using surface enhanced Raman spectroscopy, *Talanta* 221, 121552 (2021)
42. F. Qing, Y. Zhang, Y. Niu, R. Stehle, Y. Chen, and X. Li, Towards large-scale graphene transfer, *Nanoscale* 12(20), 10890 (2020)
43. S. C. Xu, J. Zhan, B. Y. Man, S. Z. Jiang, W. W. Yue, S. B. Gao, C. G. Guo, H. P. Liu, Z. H. Li, J. H. Wang, and Y. Q. Zhou, Real-time reliable determination of binding kinetics of DNA hybridization using a multi-channel graphene biosensor, *Nat. Commun.* 8(1), 14902 (2017)
44. N. Nekrasov, S. Jaric, D. Kireev, A. V. Emelianov, A. V. Orlov, I. Gadjanski, P. I. Nikitin, D. Akinwande, and I. Bobrinetskiy, Real-time detection of ochratoxin A in wine through insight of aptamer conformation in conjunction with graphene field-effect transistor, *Biosens. Bioelectron.* 200, 113890 (2022)
45. G. F. Wu, X. Tang, M. Meyyappan, and K. W. C. Lai, Doping effects of surface functionalization on graphene with aromatic molecule and organic solvents, *Appl. Surf. Sci.* 425, 713 (2017)
46. M. Tian, M. Qiao, C. C. Shen, F. Meng, L. A. Frank, V. V. Krasitskaya, T. J. Wang, X. M. Zhang, R. H. Song, Y. X. Li, J. J. Liu, S. C. Xu, and J. H. Wang, Highly-sensitive graphene field effect transistor biosensor using PNA and DNA probes for RNA detection, *Appl. Surf. Sci.* 527, 146839 (2020)
47. Y. N. Zhang, Y. Ding, C. Li, H. Q. Xu, C. X. Liu, J. J. Wang, Y. Ma, J. F. Ren, Y. F. Zhao, and W. W. Yue, An optic-fiber graphene field effect transistor biosensor for the detection of single-stranded DNA, *Anal. Methods* 13(15), 1839 (2021)
48. C. T. Lin, P. T. K. Loan, T. Y. Chen, K. K. Liu, C. H. Chen, K. H. Wei, and L. J. Li, Label-free electrical detection of DNA hybridization on graphene using Hall effect measurements: Revisiting the sensing mechanism, *Adv. Funct. Mater.* 23(18), 2301 (2013)
49. E. Sameiyan, E. Bagheri, S. Dehghani, M. Ramezani, M. Alibolandi, K. Abnous, and S. M. Taghdisi, Aptamer-based ATP-responsive delivery systems for cancer diagnosis and treatment, *Acta Biomater.* 123, 110 (2021)
50. J. Mehringer, T. M. Do, D. Touraud, M. Hohenschutz, A. Khoshsima, D. Horinek, and W. Kunz, Hofmeister versus Neuberg: is ATP really a biological hydrotrope, *Cell Rep. Phys. Sci.* 2(2), 100343 (2021)
51. S. C. Xu, C. Zhang, S. Z. Jiang, G. D. Hu, X. Y. Li, Y. Zou, H. P. Liu, J. Li, Z. H. Li, X. X. Wang, M. Z. Li, and J. H. Wang, Graphene foam field-effect transistor for ultra-sensitive label-free detection of ATP, *Sens. Actuators B Chem.* 284, 125 (2019)
52. C. M. Yu, X. M. Chang, J. Liu, L. P. Ding, J. X. Peng, and Y. Fang, Creation of reduced graphene oxide based field effect transistors and their utilization in the detection and discrimination of nucleoside triphosphates, *ACS Appl. Mater. Interfaces.* 7(20), 10718 (2015)
53. W. W. Yue, S. Z. Jiang, S. C. Xu, F. Z. Huang, and C. J. Bai, Fabrication of capacitive type biosensor based on CVD grown grapheme, Proceedings 2013 International Conference on Mechatronic Sciences, Electric Engineering

and Computer (MEC), Shenyang, China, 2013, pp 711–714

54. S. Xu, B. Man, S. Jiang, W. Yue, C. Yang, M. Liu, C. Chen, and C. Zhang, Direct growth of graphene on quartz substrates for label-free detection of adenosine triphosphate, *Nanotechnology* 25(16), 165702 (2014)
55. P. Snapp, M. Heiranian, M. T. Hwang, R. Bashir, N. R. Aluru, and S. W. Nam, Current understanding and emerging applications of 3D crumpling mediated 2D material–liquid interactions, *Curr. Opin. Solin. St M.* 24(3), 100836 (2020)
56. K. Shoorideh and C. O. Chui, On the origin of enhanced sensitivity in nanoscale FET-based biosensors, *Proc. Natl. Acad. Sci. USA* 111(14), 5111 (2014)
57. D. Y. Qi, C. Wang, Y. C. Gao, H. W. Li, and Y. Q. Wu, Heteroatom doping and supramolecular assembly promoted copper nanoclusters to be a stable & high fluorescence sensor for trace amounts of ATP determination, *Sens. Actuators B Chem.* 358, 131469 (2022)
58. M. Q. Zheng, Y. F. Kang, D. Liu, C. Y. Li, B. Zheng, and H. W. Tang, Detection of ATP from "fluorescence" to "enhanced fluorescence" based on metal-enhanced fluorescence triggered by aptamer nanoswitch, *Sens. Actuators B Chem.* 319, 128263 (2020)
59. Y. Peng, D. X. Li, R. Yuan, and Y. Xiang, A catalytic and dual recycling amplification ATP sensor based on target-driven allosteric structure switching of aptamer beacons, *Biosens. Bioelectron.* 105, 1 (2018)
60. S. Li, X. T. Zhao, X. T. Yu, Y. Q. Wan, M. Y. Yin, W. W. Zhang, B. Q. Cao, and H. Wang, Fe_3O_4 nanozymes with Aptamer-Tuned catalysis for selective colorimetric analysis of ATP in blood, *Anal. Chem.* 91(22), 14737 (2019)
61. H. Y. Zhao, L. N. Dou, J. J. Ren, M. Cui, N. Li, X. P. Ji, X. T. Liu, and C. Zhang, MOF-derived porous Co_3O_4 coupled with AuNPs and nucleic acids as electrocatalysis signal probe for sensitive electrochemical aptasensing of adenosine triphosphate, *Sens. Actuators B Chem.* 362, 131753 (2022)
62. X. Li, J. M. Yang, J. Q. Xie, B. Y. Jiang, R. Yuan, and Y. Xiang, Cascaded signal amplification via target-triggered formation of aptazyme for sensitive electrochemical detection of ATP, *Biosens. Bioelectron.* 102, 296 (2018)
63. G. E. Fenoy, E. Piccinini, W. Knoll, W. A. Marmisolle, and O. Azzaroni, The effect of Amino–Phosphate interactions on the biosensing performance of enzymatic graphene field-effect transistors, *Anal. Chem.* 94(40), 13820 (2022)